

Measurements of Core Lithium Concentration in Diverted H-mode Plasmas of NSTX

M. Podestà¹, R. E. Bell¹, A. Diallo¹, B. P. LeBlanc¹, F. Scotti¹

¹Princeton Plasma Physics Laboratory, Princeton NJ 08543 - USA

E-mail contact of main author: mpodesta@pppl.gov

Abstract. NSTX is exploring the use of lithium as plasma-facing material to handle the large power flux to the wall expected in future fusion devices. Measurements of core lithium concentration, $n_{Li}(R)$, have been performed to assess the possible contamination of the core plasma caused by lithium influx. Experimental scenarios representative of the NSTX operating space for diverted H-mode are investigated. In particular, a total of 1.3 kg of lithium was evaporated into the vessel in the 2010 NSTX experimental campaign. In spite of the fact that up to hundreds of milligrams of lithium are introduced in the vessel, n_{Li} remains insignificant in the core. Measured values $n_{Li} \ll 0.1\%$ of the electron density are rather insensitive to variations of toroidal field, plasma current, divertor conditions. No dependence on the technique utilized for lithium conditioning of the vessel wall is observed.

1. Introduction and experimental setup

Large heat fluxes impinging on the vacuum vessel wall of a fusion device can cause erosion and damage of the plasma facing components (PFCs). For example, the steady-state perpendicular heat flux to the divertor must be limited to 10 MW/m^2 for the present ITER design [1]. At the same time, the ideal material for the PFCs must not cause an excessive influx of impurities from the plasma boundary into the core. Lithium has been proposed as a candidate interface between carbon or metallic PFCs and the plasma boundary.

Techniques for lithium conditioning of the PFCs have been tested on a number of devices [2][3][4][5], including the National Spherical Torus Experiment (NSTX [6]), on which the possible benefits and drawbacks of lithium as plasma-facing material were investigated in the past years [7][8][9]. Active charge-exchange recombination spectroscopy (CHERS) measurements from 2008 indicated that n_{Li} remains small, about $\sim 0.1\%$ or less of the electron density [7]. The implementation of a new divertor configuration aimed at exploring the physics of a liquid lithium divertor (LLD) in 2010 motivated additional measurements of n_{Li} for a wider range of operating conditions. Data from the 2010 experimental campaign are used to investigate the behavior of lithium under a variety of conditions. The results indicate that lithium does not accumulate in significant amounts inside the plasma, whereas carbon, which constitutes the primary PFC material on NSTX, remains the dominant impurity [10]. Note that, because all lithium charge-exchange lines are blended with a corresponding carbon line at nearly the same wavelength, the exact quantification of n_{Li} is challenging. Hereafter, reported values of n_{Li} refer to the entire emission from the blended lines and therefore represent an upper limit.

The NSTX spherical torus has major and minor radius $R_0 = 0.85 \text{ m}$ and $a \lesssim 0.65 \text{ m}$ (aspect ratio 1.3 – 1.5) and operates with a toroidal field 3.5-5.5 kG, plasma current $\sim 1 \text{ MA}$ and deuterium as filling gas. Densities are $3 - 10 \times 10^{19} \text{ m}^{-3}$. Core electron and ion temperatures are $T_e \approx T_i \sim 1 \text{ keV}$. Neutral beam (NB) injection is the primary heating and current-drive

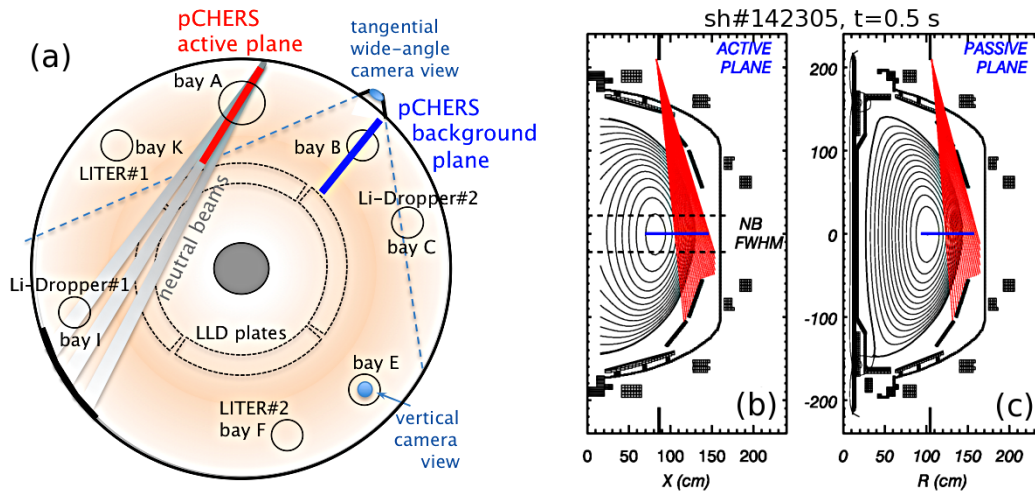


FIG. 1: (a) Top view of NSTX showing the position of the main systems used for this work. (b-c) Layout of the pCHERS views used for measurements of lithium. The active plane is shown along the path of the NB source B (coordinate X). The thick blue line at mid-plane ($Z = 0$) in each panel indicates the range covered by the main (toroidal) CHERS views.

system, with maximum available power $P_{NB} = 7$ MW and injection energies 60 – 90 keV. Although the inner wall is primarily covered by graphite tiles, a new liquid lithium divertor (LLD [11]) system was installed in 2010 on the lower divertor region. Lithium is evaporated on the PFCs from the top of the NSTX vessel prior to a discharge from two evaporators (LITERs [12]) located ≈ 180 degrees apart toroidally, see figure 1a. Typical evaporation rates are 5 – 15 mg/min for 5-10 minutes in between discharges. A second technique to introduce lithium in the NSTX vessel utilizes a lithium dropper (Li-Dropper [13]) that releases small lithium granules from the top of the machine. Two systems, located at two opposed toroidal locations, were operational on NSTX in 2010. Through the Li-Droppers, controlled quantities of lithium are introduced either before or during a discharge, contrary to the continuous LITER evaporation. The LITER and Li-Dropper (used before a discharge) deposit lithium mainly on the PFCs at the bottom of the NSTX vacuum chamber, i.e. where most of the plasma-wall interactions occur.

1.1. Diagnostic techniques for n_{Li} measurements

Several CHERS systems were available during the 2010 campaign for simultaneous measurements of carbon and lithium concentrations [10]. Each system consists of a fixed-wavelength spectrometer coupled to a Charge-Coupled Device detector with sampling rate 100 Hz. Two of the six *poloidal* systems were converted to n_{Li} measurements in the wavelength range 5145 – 5180 Å of Li III emission (rest wavelength in air $\lambda = 5166.89$ Å for the $n = 7 \rightarrow 5$ transition [14]). Light from NSTX plasmas is transported from the NSTX test-cell to a separated diagnostic room through optical fibers. Both *active* (charge-exchange) lithium emission from the region intercepting the heating NB and *passive* (or background) contributions are measured, see figure 1. The *lithium-poloidal-CHERS* (Li-pCHERS) views cover the radial range $R \approx 120 - 155$ cm. Temporal resolution is 10 ms. Other pCHERS views, tuned to C VI emission ($n = 8 \rightarrow 7$ transition at 5290.5 Å) [15], are interleaved with the Li-pCHERS views.

Large uncertainties in the inferred n_{Li} are caused by the C VI line ($n = 14 \rightarrow 10$ transition, $\lambda = 5166.67$ Å) located at the same wavelength as the Li III line of interest. The resulting blend in the measured spectrum is further broadened by the instrumental function of the spectrometer. A quantitative estimate of the relative brightnesses from Li III and C VI is obtained by fitting

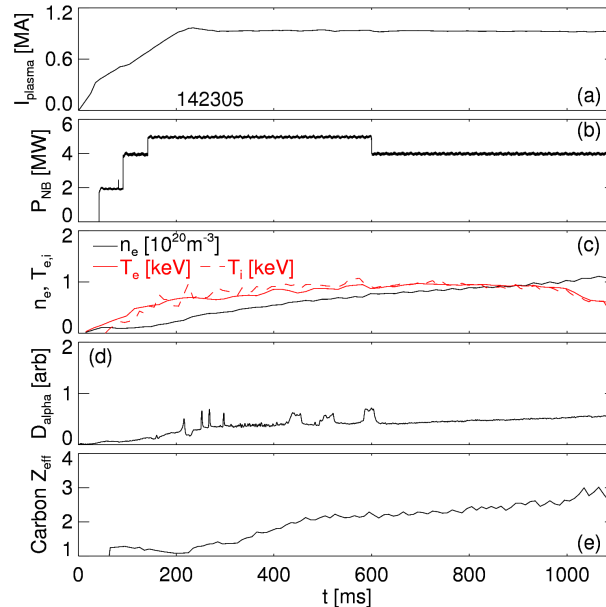


FIG. 2: Main parameters for shot no. 142305: (a) plasma current, (b) injected NB power; (c) central electron density and ion/electron temperature, (d) D-alpha emission from the divertor. (e) Core Z_{eff} , calculated from *CHERS* under the assumption of carbon as the dominant impurity.

the lines around 5167 \AA under the assumptions that the two species are in thermal equilibrium with temperature T_i [10]. The results of this procedure indicate that $\approx 50\%$ of the measured brightness is due to carbon, although the exact carbon fraction is difficult to quantify. For practical purposes, the entire emission of the active signal will be treated as being only from lithium hereafter and values of lithium density must then be interpreted as upper limits rather than exact values. The relative brightness from Li III is finally re-scaled, based on the C VI emission measured by the carbon p*CHERS* and the absolutely calibrated C VI emission from the main (toroidal) *CHERS*. It should be noted that Li data are representative of line-integrated measurements. Comparison with inverted profiles [15] for a limited number of discharges indicates that line-integrated measurements capture the general features of lithium evolution, such as average concentration and trends with plasma parameters [10].

2. Li concentration in H-mode, NB-heated plasmas

A set of discharges from the 2010 campaign are chosen as representative of the NSTX operating space for H-mode diverted plasmas. Preference is given to sequences where only a few parameters are varied in a systematic way. Discharges with injected NB power $2 \leq P_{NB} \leq 4 \text{ MW}$ have been preferentially selected to minimize MHD activity, since strong MHD activity causes non-reproducibility among discharges. A NSTX discharge with plasma current $I_{plasma} = 0.9 \text{ MA}$ and toroidal field on axis $B_{tor} = 4 \text{ kG}$ is shown in figure 2. The injected NB power is $P_{NB} = 4 - 6 \text{ MW}$. A phase with relatively stationary plasma parameters starts after the transition in H-mode at $t \approx 210 \text{ ms}$. Core T_e and T_i are $\lesssim 1 \text{ keV}$. As often observed in discharges with large lithium evaporation rates, edge-localized modes (ELMs) are not de-stabilized, as deduced from the lack of spikes in the edge D-alpha emission (figure 2d) [16]. As a drawback, the impurity content in the plasma continues to increase, as inferred from the effective charge Z_{eff} (figure 2e). Values of Z_{eff} are calculated here assuming that carbon is the dominant low- Z impurity, which is usually verified for NSTX plasmas. The temporal evolution of lithium and carbon densities for the discharge in figure 2 is shown in figure 3. The profiles starts to build up

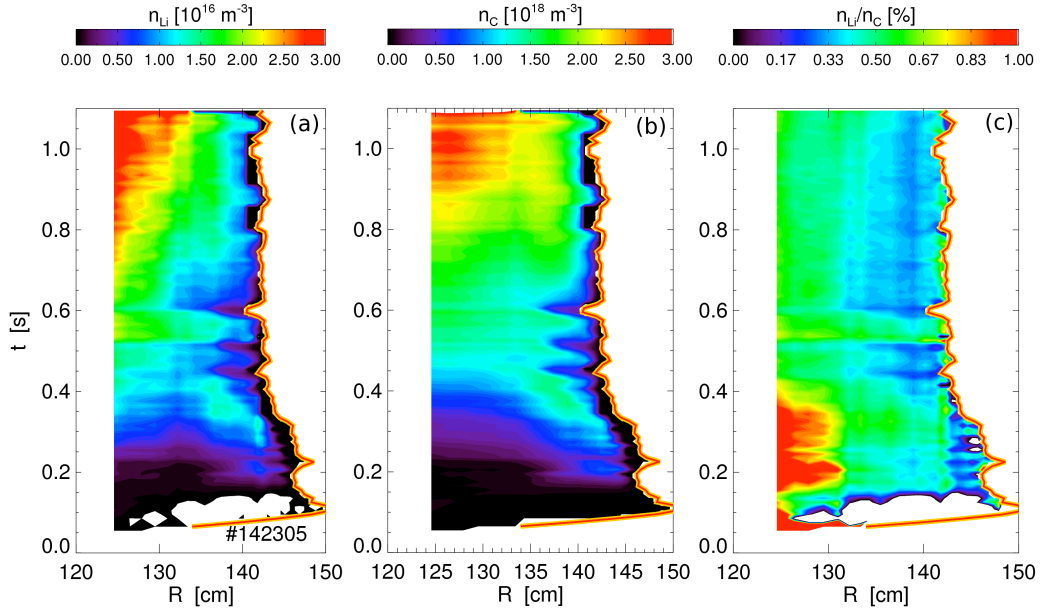


FIG. 3: Lithium (a) and carbon (b) densities (from line integrated data). (c) Ratio of lithium to carbon concentrations. Data refer to NSTX discharge no. 142305, see figure 2. The red line indicates the radius of the separatrix at midplane, as calculated through the equilibrium code EFIT.

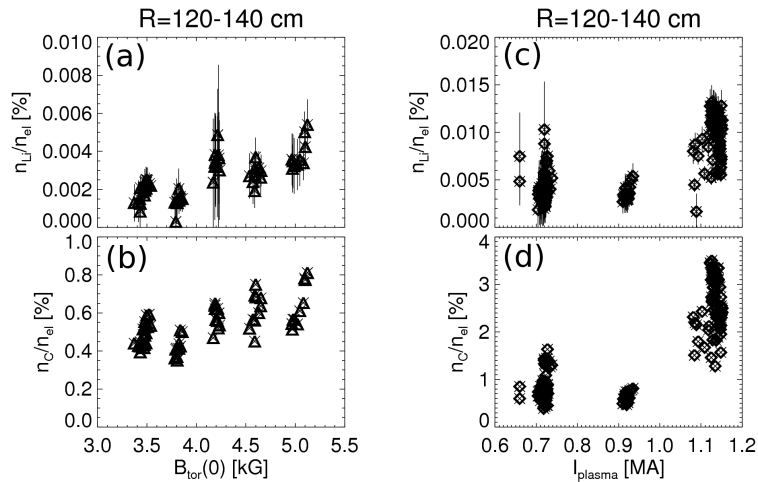


FIG. 4: Lithium (a-b) and carbon (c-d) concentrations as a function of toroidal field for fixed $I_{plasma} = 0.9$ MA (left column) and of plasma current for fixed $B_{tor} = 5.5$ kG (right column). Measurements shown here are from $t = 250 - 400$ ms.

after the transition to H-mode. Nevertheless, the absolute lithium density is low compared to both deuterium and carbon densities. Lithium concentration remains below 2% of the carbon density and $\ll 0.1\%$ of the electron density during the entire discharge (figure 3b).

2.1 . Scan of toroidal field, plasma current and aspect ratio

The observations from figure 3 are confirmed by the results show in figure 4 for two scans of B_{tor} and I_{plasma} . In addition, a slight increase of the average impurity content with increasing B_{tor} and I_{plasma} is inferred, which is consistent with a general improvement of confinement [17]. For devices with higher field than NSTX, such as the planned NSTX-U [18], this unfavor-

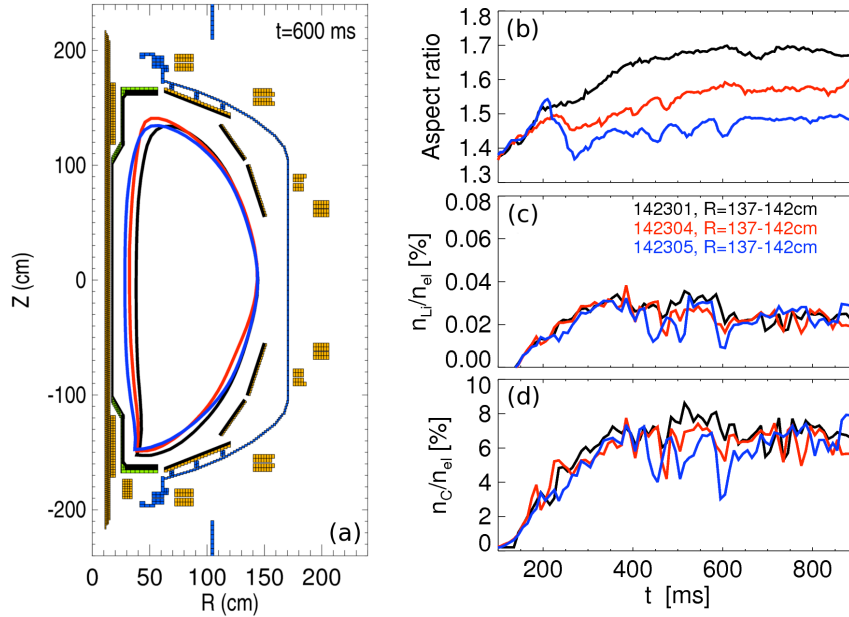


FIG. 5: (a) Cross-section of NSTX with plasma separatrix at $t = 600$ ms, corresponding to the flat-top, stationary phase. (b) Time evolution of aspect ratio. The plasma configuration is the same for all four discharges up to the end of the current ramp-up at $t = 200$ ms, then is varied during the current flat-top. (c-d) Ratio of lithium and carbon concentrations over electron density.

able scaling, leading to larger impurity accumulation, needs to be addressed, *cf.* Refs. [19][20].

A third parameter of interest for projections of NSTX results to future devices is the aspect ratio. For instance, the planned NSTX upgrade implies a larger center column, leading to larger aspect ratio for standard configurations. Larger aspect ratios are obtained on NSTX by shifting the plasma outward, away from the center column. A comparison of impurity content as a function of aspect ratio is shown in figure 5 for three discharges. The aspect ratio is varied from ~ 1.4 (typical of NSTX plasmas) up to ~ 1.7 (projected value for NSTX-U), see figure 5b. Note that the plasma elongation (not shown) also changes with the aspect ratio. No substantial changes of the lithium core concentration are measured when the aspect ratio is varied (figures 5c-d), suggesting that the influx of impurities due to enhanced sputtering from the center stack tiles does not depend on the inner gap size. Another observation is that the three discharges follow a similar trajectory during the start-up and ramp-up phases, up to $t \approx 200$ ms, after which the aspect ratio is varied to achieve the desired value during the current flat-top. This may indicate that rather large impurity accumulation occurs during the initial evolution of the discharge and is then maintained during the flat-top phase.

2.2. Li concentration for different Li conditioning techniques

In principle, different techniques to introduce lithium in the vessel may be associated with different impurity source terms, that affect the accumulation of lithium (and carbon) in the plasma core. To test this hypothesis, four discharges are compared with different amounts of lithium evaporated from LITER or injected through the Li-Dropper, see table I. Plasma parameters and magnetic configuration are nearly the same for the four discharges. A camera view of the plasma during lithium injection from the Li-Dropper confirms that lithium granules do interact with the edge plasma, see figure 6a. Nevertheless, similar values of n_{Li} are measured for discharges with lithium from LITER prior to the shot, with lithium from the Li-Dropper or

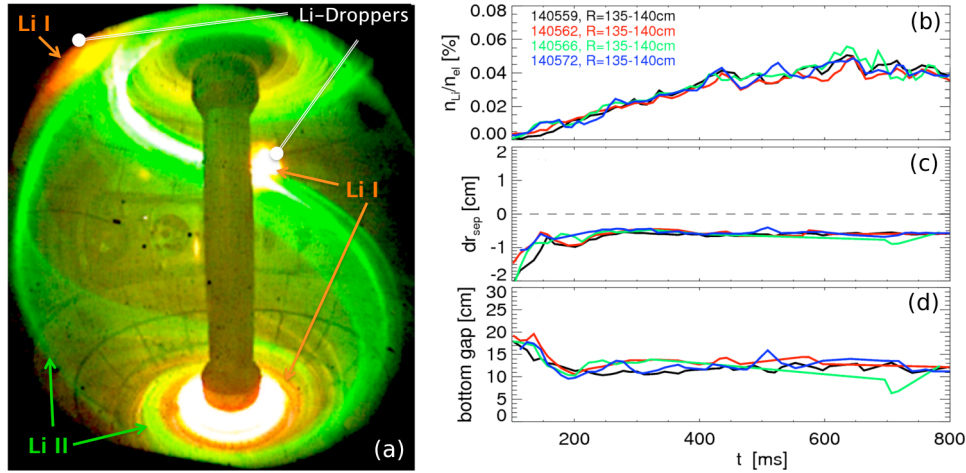


FIG. 6: Mid-plane camera view of NSTX (cf. figure 1a) for discharge no. 140572. Both Li-Dropper systems are releasing lithium during the shot. Emission from Li I (red) and Li II (green) are clearly visible. Time evolution of (b) ratio of lithium to electron concentrations, (c) vertical displacement from mid-plane (dr_{sep}) and (d) bottom gap for similar discharges with different amounts of lithium from LITER and Li-Droppers, see Table I.

with both together (figure 6b). Carbon concentration does not vary significantly among the different discharges. Because lithium conditioning of the PFCs has some cumulative effect if LITER is used for many consecutive discharges, it is conjectured that the dominant lithium reservoir is still constituted by evaporated lithium from LITER that has accumulated on the PFCs from previous shots rather than by instantaneous injection from the Li-Dropper.

2.3. Li concentration during anomalous events

From the previous Sections, it is concluded that the core n_{Li} on NSTX remains small, $\lesssim 0.1\%$ of the carbon concentration, regardless of the details of the discharge. Special events are the only exception that can lead to relatively large (for NSTX) n_{Li} . An example of anomalous event directly associated with lithium is the interaction of the plasma with a macroscopic conglomerate of lithium that accidentally fell on the lower divertor plate from the LITER port. The footprint of the lithium piece has a surface of a few square centimeters. The evolution of lithium concentration, shown in Fig. 7, is similar to what already discussed in figure 3 up to ≈ 300 ms, when the outer strike point moves on the lithium conglomerate. At this time, lithium concentration starts to increase transiently, with a burst of lithium observed at $t \approx 320$ ms. Finally, a disruption causes the termination of the discharge. The maximum estimated lithium concentration is $n_{Li}/n_e \gtrsim 0.2\%$, with $n_{Li}/n_C \gtrsim 25\%$ and $n_C/n_e \sim 1\%$.

TABLE I: Total amounts of lithium deposited from LITER and Li-Dropper for the discharges in figure 6. For the Li-Dropper, the first value in the sum refers to the amount of lithium pre-positioned before the discharge and the second value to the amount released during the discharge.

| shot no. | LITER | Li-Dropper |
|----------|--------|----------------------------------|
| 140559 | 240 mg | — |
| 140562 | 240 mg | 240 mg + 240 mg/s \times 1.2 s |
| 140566 | 240 mg | 0 mg + 100 mg/s \times 1.1 s |
| 140572 | 120 mg | 240 mg + 120 mg/s \times 1.2 s |

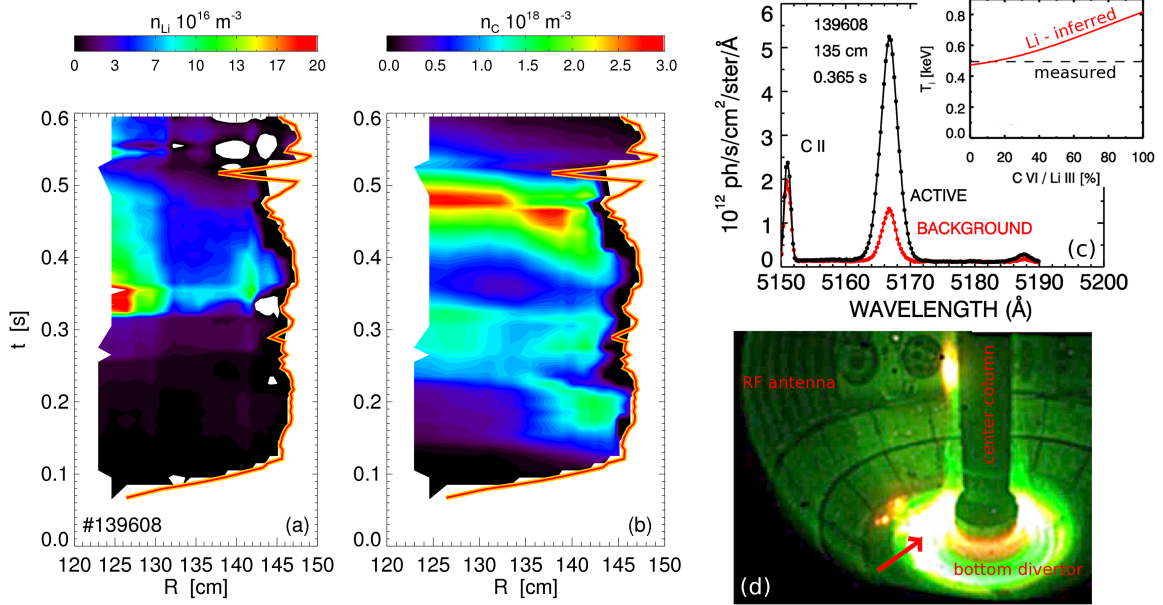


FIG. 7: (a-b) Lithium and carbon densities for discharge no. 139608. (c) Spectrum at $t \sim 365$ ms showing anomalously large brightness attributed to lithium, according to a fit with constrained T_i (cf. pag. 2). (d) Camera image of visible light at $t \sim 370$ ms. Plasma interacts with a macroscopic fragment of lithium on the lower divertor (red arrow).

3. Conclusions

Dedicated charge-exchange recombination spectroscopy measurements throughout the 2010 NSTX experimental campaign indicate that extremely low core lithium concentrations are a robust property of NSTX plasmas. A slight increase in the average impurity concentration is observed when either the magnetic field or the plasma current are increased, consistently with an improvement in confinement. In spite of the potentially different conditions induced at the plasma-PFC interface when lithium is inserted via different techniques (LITER, Li-Dropper), no substantial variations are measured in the core lithium concentration. A large increase of n_{Li} is only observed during transient, anomalous events such as the plasma interaction with a macroscopic conglomerate of lithium located on the lower divertor. In this case n_{Li} is larger than in typical NSTX plasmas, but its effects on plasma contamination remain very modest. For instance, $n_{Li}/n_e \sim 0.2\%$ would cause an increase in Z_{eff} of only $\Delta Z_{eff} \approx 0.012$.

In conclusion, n_{Li} remains extremely low in the core plasma of NSTX, even after a large amount of lithium, of the order of hundreds of milligrams, is evaporated on the PFCs. Upper limits from experimental data are $\ll 0.1\%$ of the electron density from the plasma mid-radius ($R \approx 120$ cm) out to the edge ($R = 140 - 145$ cm). Consistently with previous results [7], carbon remains the dominant impurity for NSTX plasmas.

Acknowledgments

The authors would like to thank Drs. S. A. Sabbagh and J. E. Menard for the equilibrium reconstructions used in this work. The contribution of the NSTX NBI group and the LITER/Li-Dropper operators is gratefully acknowledged. Work supported by DOE grant no. DE-AC02-09CH11466.

-
- [1] LOARTE, A. et al., ITER physics basis, chapter 4: Power and particle control, *Nuclear Fusion* **47** (2007) S203.
- [2] MANSFIELD, D. K. et al., Observations concerning the injection of a lithium aerosol into the edge of TFTR discharges, *Nucl. Fusion* **41** (2001) 1823.
- [3] MIRNOV, S. V. et al., Li-CPS limiter in tokamak T-11M, *Fusion Eng. Des.* **65** (2003) 455.
- [4] MAZZITELLI, G. et al., FTU results with a liquid lithium limiter, *Nucl. Fusion* **51** (2011) 073006.
- [5] SÁNCHEZ, J. et al., Impact of lithium-coated walls on plasma performance in the TJ-II stellarator, *J. Nucl. Mater.* **390-391** (2009) 852.
- [6] ONO, M. et al., Exploration of spherical torus physics in the NSTX device, *Nucl. Fusion* **40** (2000) 557.
- [7] BELL, M. G. et al., Plasma response to lithium-coated plasma-facing components in the national spherical torus experiment, *Plasma Phys. and Control. Fusion* **51** (2009) 124054.
- [8] MAINGI, R. et al., Continuous improvement of H-mode discharge performance with progressively increasing lithium coatings in the National Spherical Torus Experiment, *Phys. Rev. Lett.* **107** (2011) 145004.
- [9] ONO, M. et al., Recent progress of NSTX lithium program and opportunities for magnetic fusion research, *Fusion Eng. Des.* (2011) <http://dx.doi.org/10.1016/j.fusengdes.2011.10.011>.
- [10] PODESTÀ, M. et al., Measurements of core lithium concentration in a Li-conditioned tokamak with carbon walls, *Nucl. Fusion* **52** (2012) 033008.
- [11] KUGEL, H. W. et al., NSTX plasma operation with a Liquid Lithium Divertor, *Fusion Eng. Des.* (2011) <http://dx.doi.org/10.1016/j.fusengdes.2011.07.010>.
- [12] KUGEL, H. W. et al., Lithium coatings on NSTX plasma facing components and its effects on boundary control, core plasma performance, and operation, *Fusion Eng. Des.* **85** (2010) 865.
- [13] MANSFIELD, D. K. et al., A simple apparatus for the injection of lithium aerosol into the scrape-off layer of fusion research devices, *Fusion Eng. Des.* **85** (2010) 890.
- [14] Wavelengths of spectral lines from Atomic Line List, <http://www.pa.uky.edu/~peter/atomic>.
- [15] BELL, R. E. et al., Comparison of poloidal velocity measurements to neoclassical theory on NSTX, *Phys. Plasmas* **17** (2010) 082507.
- [16] MAINGI, R. et al., Edge-localized-mode suppression through density-profile modification with lithium-wall coatings in the National Spherical Torus Experiment, *Phys. Rev. Lett.* **103** (2009) 075001.
- [17] KAYE, S. M. et al., Confinement and local transport in the National Spherical Torus Experiment (NSTX), *Nucl. Fusion* **47** (2007) 499.
- [18] MENARD, J. E. et al., Overview of the physics design and engineering of NSTX upgrade, *Nucl. Fusion* **52** (2012) 083015.
- [19] SOUKHANOVSKII, V. A. et al., Taming the plasma-material interface with the snowflake divertor in NSTX, *Nuclear Fusion* **51** (2011) 012001.
- [20] CANIK, J. M. et al., Progress in the development of ELM pace-making with non-axisymmetric magnetic perturbations in NSTX, *Nucl. Fusion* **50** (2010) 064016.